A MESO-α-SCALE STUDY OF MEIYU FRONT HEAVY RAIN—PART II: THE DYNAMICAL ANALYSIS OF RAIN-BAND DISTURBANCE

Yang Guoxiang (杨国祥), *Lu Hancheng* (陆汉城) and *He Qiqiang* (何齐强)

Institute of Meteorology, PLA Air Force, Nanjing

Received 21 February, 1986

ABSTRACT

The alternating change of the two meiyu front rain-bands caused by the alternating change between the moist potential vorticities is discussed. The main factors of the change of moist potential vorticity are the vertical and horizontal divergence of moist potential vorticity flux as well as the vertical transport caused by the cumulus mass flux. Also discussed is the possibility that the WAVE-CISK conditional symmetric instability in the baroclinic moist atmosphere leads to the forming of the double rain-bands and their roller-shaped circulation features. Theoretical analyses show that the latitudinal disturbance scale-selection by the primitive moisture model of the latent heat release in cumulus convection depends on the stratification instability parameter (Ri number) and viscous coefficient of eddy.

I. INTRODUCTION

Part I of this paper has revealed the meiyu front rain-band structure and its circulation characteristics. Within a single meso-α-scale rain-band, several heavy rain-clusters are often found to be active one after another and the meso-β-scale disturbance associated with the heavy rain clusters is characteristic of gravitational wave. When several rain-bands are present, the circulations at the middle-and low-level are roller-shaped with their axes parallel to the rain-bands, but at the high-level they are indirect circulations.

Many observations and studies of the extratropical cyclonic front system (e.g. Elliott and Hovind 1964, 1965; Nozumi and Arakawa, 1968; Browning and Harrold, 1969; Kreitzburg and Browning, 1970) have shown that the frontal cloud and precipitation are concentrated in the area parallel to the front and the length of rain-band is much longer than the interval of 80–300 km between the rain-bands; the cause of the formation of these rain-bands may be the Ekman layer instability in the frontal zone, the gravitational wave produced on the front and the conditional symmetric instability (Bennetts, 1979), and so on.

As indicated in Part I, the meso-α-scale rain-bands in the meiyu front in East China are characteristic of the similar conditional symmetric instability which forms the roller-shaped circulations. Therefore, we use the WAVE-CISK conditional symmetric instability in the baroclinic moist atmosphere to study the cause of the generation of meiyu frontal precipitation bands in East China. Before the theoretical study it is necessary to diagnoze the intensity change of the rain-bands with moist potential vorticity, because it is an important characteristic value in expressing the properties of the atmospheric thermodynamics and atmospheric dynamics. Bennetts (1979) proposed that the necessary condition of the instability

in the conditional symmetric atmosphere be $q<0$, $\left[q=\frac{gf}{\theta_0}\left(f-\frac{\partial v}{\partial x}\right)\frac{\partial\theta}{\partial z}-\frac{g^2}{\theta_0^2}\left(\frac{\partial\theta}{\partial x}\right)^2\right]$, q is directly proportional to the Ertel potential vorticity. He also pointed out that the atmosphere can not be symmetrically unstable without friction and heat source. The analysis of potential vorticity in the moist atmosphere contribute to understanding the cause of the instability in the meiyu front season. Wang Yongzhong et al. (1984) have applied the diagnosis of potential vorticity to the study of heavy rain and have pointed out that there is a close relationship between the vorticity and the development of heavy rain. So the diagnosis of moist potential vorticity is useful for us to discuss the development of rain-bands and the alternating change in intensity between the double rain-bands.

II. DIAGNOSIS OF MOIST POTENTIAL VORTICITY

The moist potential vorticity Q defined in this paper is equal to $(-\partial\theta_{se}/\partial P)\cdot(\zeta+f)$. Since the meiyu front is a phenomenon in the lower atmosphere, with convergence lines at the middle- and low-level, the calculations of the moist potential vorticity at 850 hPa are of evident physical significance. As shown in Fig. 1, taking the difference in the vertical direction, the time difference is $\Delta t=3$ hours. As the middle latitude geostrophic vorticity is generally

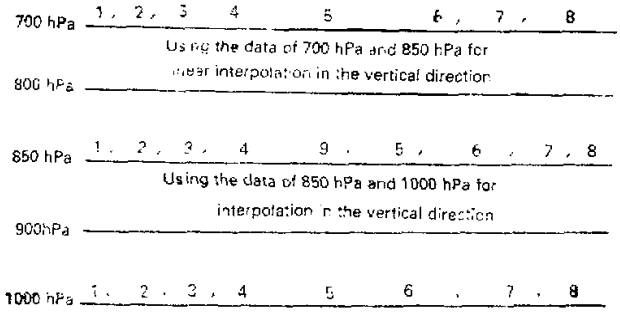

Fig. 1. The vertical difference scheme of moist potential vorticity diagnosis
1-u; 2-v; 3-w; 4-θ_{se}; 5-$\Delta\theta_{se}/\Delta t$; 6-$\vec{v}\cdot\nabla\theta_{se}$;
7-H_R; 8-M_C; 9-$-\Delta\theta_{se}/\Delta p$.

greater than the relative vorticity, the direct calculation of horizontal distribution of $\zeta(-\partial\theta_{se}/\partial P)$ can further reveal the matching relationship between the precipitation region and the moist potential vorticity. The calculation of meiyu front precipitation of 27 June 1981 shows that before the northern rain-band had appeared, there was a strong negative, relative potential vorticity (Fig. 2). While the northern rain-band arose and developed, it became weaker and finally positive (Fig. 3) when the northern rain-band reached its climax, which resulted from the forming and developing of precipitation band, and the unstable energy release which led to the lessening of stratification instability or cyclonic vorticity. The fact that the stratification tended to be neutral or stable accounts for the relative potential vorticity in the southern rain-band, of which the maintaining time is longer, keeping positive or slightly negative.

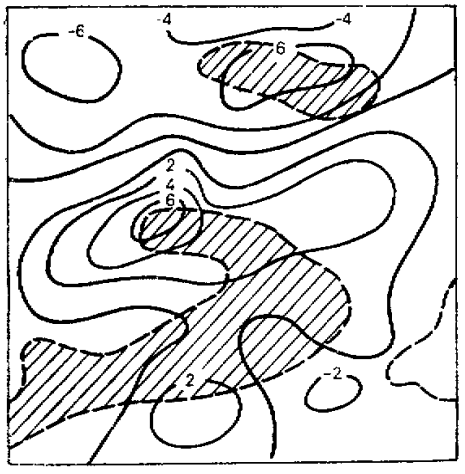

Fig. 2. The disposition of the relative potential vorticity at 0200Z June 27 and the rain-band in 0200–0400Z.

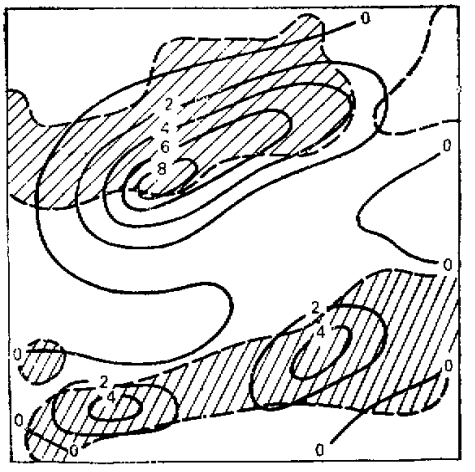

Fig. 3. The disposition of the relative potential vorticity at 0800Z June 27 and the rain-band in 0800–1000Z.

Now, let us analyze the relationship between the rate of change of the moist potential vorticity and the rain-bands through the following equation of moist potential vorticity in X, Y, P, t coordinates (Yang, 1981):

$$\frac{\partial}{\partial t}(\bar{\Gamma}_d\bar{Q}) = -\nabla\cdot(\vec{V}\bar{\Gamma}_d\bar{Q}) - \frac{\partial}{\partial p}(\bar{\omega}\bar{\Gamma}_d\bar{Q}) + \bar{Q}\frac{\partial\vec{V}}{\partial p}\cdot\nabla\bar{\theta}_{se} - \bar{\Gamma}_d\left(\frac{\partial\bar{\omega}}{\partial x}\frac{\partial\bar{v}}{\partial p} - \frac{\partial\bar{\omega}}{\partial y}\frac{\partial\bar{u}}{\partial p}\right)$$

(1) (2) (3) (4)

$$-\frac{\partial}{\partial p}(\bar{Q}M_c\bar{\Gamma}_d) - \frac{\bar{Q}}{C_p}\left[\frac{\partial}{\partial p}\left(\frac{p_0}{p}\right)^{R/C_p}H_R\right] - \bar{\Gamma}_d\left(\frac{\partial F_y}{\partial x} - \frac{\partial F_x}{\partial y}\right)$$

(5) (6) (7)

$$-\bar{\Gamma}_d\left(\frac{\partial M_c}{\partial x}\frac{\partial\bar{v}}{\partial p} - \frac{\partial M_c}{\partial y}\frac{\partial\bar{u}}{\partial p}\right)$$

(8)

where "–" represents the quantity of grid scale; $\bar{\Gamma}_d = -\frac{\partial\theta_{se}}{\partial p}$, $\bar{Q} = \bar{\zeta} + f$, $\bar{H}_R$ are the radiant heating rates of unit mass air respectively; M_c is cumulus mass flux; and the rest are equal to those common signs. On the left is the change rate of moist potential vorticity, and on the right:

(1) the horizontal divergence of moist potential vorticity flux;
(2) the vertical divergence of moist potential vorticity flux;
(3) the effects of vertical wind shear and potential equivalent temperature gradient;
(4) the twisting effect;
(5) the vertical convergence of moist potential vorticity caused by cumulus mass flux of sub-grid scale;
(6) the vertical difference of radiation effect;

(7) the frictional effect;

(8) the lateral difference of cumulus mass flux under the vertical wind shear.

The M_c parameterization scheme is the same with that of Yang (1981), i.e.

$$M_c=\left[-\frac{\partial\bar{\theta}_{se}}{\partial t}-\bar{\vec{V}}\cdot\nabla\bar{\theta}_{se}+\bar{\omega}\frac{\partial\bar{\theta}_{se}}{\partial p}-\frac{1}{C_p}\left(\frac{p_0}{p}\right)^{R/C_p}\bar{H}_R\right]\Big/\left(-\frac{\partial\bar{\theta}_{se}}{\partial p}\right).$$

The heat radiation scheme is after Zhu (1979). The results of our diagnoses show that the order of magnitude of the change rate of moist potential vorticity caused by the radiant heating and the frictional effect is less than 10^{-12}, one order less than the other terms, and therefore is negligible (the obtained net radiant heating rate is about 1°C per day; the drag coefficient is 2.5×10^{3}).

In order to display further the total effect of each term's factor, the mean of each absolute value in the experiment region has been calculated individually, which reflects that at different stage of rain-band development, each factor acts a different part. During the arising and developing period of rain-bands, terms (1), (2), (5) and (8) played an important role, while after the climax of rain-bands only terms (5) and (8) played an important role.

To describe the relationship between the change rate of moist potential vorticity and the development of rain-bands, the change of each factor's mean value with time (by taking the mean value of the grid point of the northern and southern rain-bands) is given as follows:

Table 1. The Change Rate of Moist Potential Vorticity at 850 hPa and Its Component. (10^{11}°C/S^2 hPa)

Time	0200Z		0500Z		0800Z		1100Z	
Rain-Band	N	S	N	S	N	S	N	S
$-\nabla\cdot(\bar{\vec{V}}\bar{Q}\bar{\Gamma}_d)$	14.3	− 7.0	9.9	− 7.6	3.1	− 1.0	−12.6	− 0.3
$-\frac{\partial}{\partial p}(\bar{\omega}\bar{Q}\bar{\Gamma}_d)$	−13.4	14.7	−11.1	7.3	6.9	− 5.2	12.2	21.1
$\bar{Q}\left(-\frac{\partial\bar{\vec{V}}}{\partial p}\cdot\nabla\bar{\theta}_{se}\right)$	− 4.6	− 4.1	− 4.4	− 1.5	− 3.0	19.4	1.5	25.2
$-\bar{\Gamma}_d\left(\frac{\partial\bar{\omega}}{\partial x}\frac{\partial\bar{v}}{\partial p}-\frac{\partial\bar{\omega}}{\partial y}\frac{\partial\bar{u}}{\partial p}\right)$	− 2.1	− 1.5	0.8	1.3	− 1.7	−14.5	4.4	− 2.0
$-\frac{\partial}{\partial p}(\bar{Q}M_c\bar{\Gamma}_d)$	33.0	− 7.0	45.8	12.5	3.1	19.2	1.2	−39.1
$-\bar{\Gamma}_d\left(\frac{\partial M_c}{\partial x}\frac{\partial\bar{v}}{\partial p}-\frac{\partial M_c}{\partial y}\frac{\partial\bar{u}}{\partial p}\right)$	5.7	10.7	− 4.4	− 5.7	5.9	57.4	−33.2	−30.8
$\frac{\partial}{\partial t}(\bar{\Gamma}_d\bar{Q})$	32.6	3.4	36.5	6.3	14.3	66.4	−26.2	−25.9

The precipitation area in the above table is the rain-band of 3 hours after each corresponding time. It can be seen that, during the development of the northern rain-band (0200–0500 Z), the main factor affecting the change rate of moist potential vorticity is the horizontal convergence (14.3) and the vertical divergence (−13.4) of moist potential vorticity as well as the

vertical flux convergence (33.0) caused by M_c. Moreover, the total rate of change during this period is convergent with greater value (32.6). After the intensified period of the northern rain-band, the three factors' role gradually becomes less important (14.3 at 0800Z) and the total change rate of moist potential vorticity becomes divergent (-26.2 at 1100Z) when the northern rain-band disappears.

As for the southern rain-band, the factors affecting the change rate of moist potential vorticity are the terms caused by the M_c horizontal difference and vertical wind shear, besides the three terms mentioned above. When the southern rain-band is maintaining with less change, the total change rate of moist potential vorticity is slightly convergent (3.4), and it increases abruptly (66.4) only in the intense stage of the rain-band and becomes divergent (-25.9) when the rain-band declines.

The convergence of the total change rate of moist potential vorticity is large in the developing period of the northern rain-band, while it is small in the southern rain-band; the convergence of the southern rain-band increases when the rain-band is intensified, while the change rate of moist potential vorticity in the northern rain-band decreases; all these demonstrate that the alternating change in the intensity of the southern and the northern rain-bands is closely related to that of the total change rate of moist potential vorticity.

What is especially significant is the contrary effects between the convergence and the divergence of moist potential vorticity flux in the horizontal and vertical directions in the southern and the northern rain-bands: there are the horizontal divergence and the vertical convergence of moist potential vorticity flux in the southern rain-band while the horizontal convergence and the vertical divergence in the northern rain-band; what is more, the effects of the M_c vertical flux transport in the southern and the northern rain-bands are almost contrary. In this sense, it can be considered that the change of moist potential vorticity in the southern rain-band excites that of the northern rain-band and then the development of the rain-band. This kind of convergent and divergent distribution of moist potential vorticity constitutes a structure similar to a secondary circulation. The diagram is as follows:

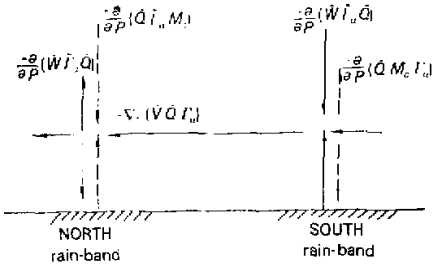

Fig. 4. The diagram of convergence and divergence of moist potential vorticity with the components of three terms.

The above analysis shows that the change rate of moist potential vorticity and its components contribute, to a degree, to the alternating change between the southern and the northern rain-bands, and thus it is of evident importance for weather forecasting to study the change of moist potential vorticity.

III. WAVE-CISK CONDITION SYMMETRIC INSTABILITY

The alternating change of the rain-bands in meiyu front is characteristic of the wave motion, which propagates along the longitudinal direction and is of meso-α-scale. In Part I, the baroclinicity of meiyu front has been analyzed and the properties of gravitational wave in the moving rain-clusters within the rain-bands has been pointed out. Therefore, we are going to discuss the development of the meso-α-scale disturbance in meiyu front with the WAVE-CISK conditional symmetric instability in the baroclinic moist atmosphere.

1. *Model Equations and Elementary Assumptions*

The ageostrophic, non-static equations of the viscous and moist atmosphere with the inherent release of latent heat of cumulus convection are as follows:

$$\frac{du}{dt}=-\frac{1}{\rho}\frac{\partial p}{\partial x}+fv+\nu\nabla^2 u, \tag{1}$$

$$\frac{dv}{dt}=-\frac{1}{\rho}\frac{\partial p}{\partial y}-fu+\nu\nabla^2 v, \tag{2}$$

$$\frac{dw}{dt}=-\frac{1}{\rho}\frac{\partial p}{\partial z}-g+\nu\nabla^2 w, \tag{3}$$

$$\frac{\partial u}{\partial x}+\frac{\partial v}{\partial y}+\frac{\partial w}{\partial z}=0, \tag{4}$$

$$\frac{d\theta_{se}}{dt}=\frac{\theta_{se}}{C_pT}\frac{dQ}{dt}+\kappa\nabla^2\theta_{se}. \tag{5}$$

ν and κ are the coefficients of eddy viscosity and diffusion respectively. Let $\nu=\kappa$, and the parameters of meiyu atmosphere are assumed as follows:

$$S^2=-f\bar{U}_z,\quad S_{Se}^2=\frac{g}{\bar{\theta}_{se}}\frac{\partial\bar{\theta}_{se}}{\partial y},\quad N_{Se}^2=\frac{g}{\bar{\theta}_{se}}\frac{\partial\bar{\theta}_{se}}{\partial z},\quad F^2=f\eta=f(f-\bar{U}_y).$$

The above parameters are taken as constants in the solving processes and the sign "–" represents the physical quantities of basic flow. Allowing for the symmetry of disturbance, we let $\frac{\partial}{\partial x}=0$.

In linearizing (1)–(5), assume $u=\bar{U}(y,z)+u'$, $v=v'$, $w=w'$. After taking Boussinesq approximation of the moist atmosphere, $\frac{\rho'}{\rho_0'}=-\frac{\theta_{Se}'}{\bar{\theta}_{se}}$ and introducing $V'=-\frac{\partial\psi}{\partial z}$, $w'=\frac{\partial\psi}{\partial y}$, we get the equations of the disturbance as follows:

$$\left(\frac{\partial}{\partial t}-\nu\nabla^2\right)u'=-\eta\frac{\partial\psi}{\partial z}-\bar{U}_z\frac{\partial\psi}{\partial y}, \tag{6}$$

$$-\left(\frac{\partial}{\partial t}-\nu\nabla^2\right)\frac{\partial\psi}{\partial z}=-\frac{1}{\rho_0}\frac{\partial p'}{\partial y}-fu', \tag{7}$$

$$\left(\frac{\partial}{\partial t}-\nu\nabla^2\right)\frac{\partial\psi}{\partial y}=-\frac{1}{\rho_0}\frac{\partial p'}{\partial z}+\frac{\theta'_{se}}{\bar{\theta}_{se}}g, \tag{8}$$

$$\left(\frac{\partial}{\partial t}-\nu\nabla^2\right)\frac{\theta'_{se}}{\bar{\theta}_{se}}g=-N^2_{se}\frac{\partial\psi}{\partial y}+S^2_{se}\frac{\partial\psi}{\partial z}+Q^*, \tag{9}$$

where $Q^*=\frac{g}{C_p\bar{T}}\frac{dQ}{dt}$. The equations (6)–(9) are turned into the equation of stream function of disturbance:

$$\left(\frac{\partial}{\partial t}-\nu\nabla^2\right)^2\left(\frac{\partial^2}{\partial y^2}+\frac{\partial^2}{\partial z^2}\right)\psi=-N^2_{se}\frac{\partial^2\psi}{\partial y^2}+(S^2+S^2_{se})\frac{\partial^2\psi}{\partial y\partial z}-F^2\frac{\partial^2\psi}{\partial z^2}+\frac{\partial Q^*}{\partial y}.$$

The WAVE-CISK parameterizing scheme of Emanual (1981), $Q^*=N^2_{se}Q_0G(z)\left(\frac{\partial\psi}{\partial y}\right)_{z=z_0}$ has been adopted, where Q_0 is proportional to the constant which indicates the cumulus convective instability, $G(z)$ is the function of vertical heating distribution and can be represented by an experimental or observational value. Let $D=\frac{\partial}{\partial t}-\nu\nabla^2$ and we obtain

$$D^2\left(\frac{\partial^2}{\partial y^2}+\frac{\partial^2}{\partial z^2}\right)\psi=-N^2_{se}\frac{\partial^2\psi}{\partial y^2}+(S^2+S^2_{se})\frac{\partial^2\psi}{\partial y\partial z}-F^2\frac{\partial^2\psi}{\partial z^2}+N^2_{se}Q_0G(z)\left(\frac{\partial^2\psi}{\partial z^2}\right)_{z=z_0}. \tag{10}$$

2. *Discussion of the Disturbance Instability*

Assume: $\psi=e^{i\sigma t}e^{ik(y\sin\phi+z\cos\phi)}$, where ϕ is an angle contained by the disturbance displacement and the horizontal replacement. Let $z=z_0$ that is then substituted into (10), and we have

$$\begin{aligned}\sigma^2-2i\nu k^2\sigma-\nu^2k^4&=[1-Q_0G(z_0)]N^2_{se}\sin^2\phi-(S^2+S^2_{se})\sin\phi\cos\phi+F^2\cos^2\phi\\&=N^2_{se1}\sin^2\phi-(S^2+S^2_{se})\sin\phi\cos\phi+F^2\cos\phi,\end{aligned}$$

where $N^2_{se1}=[1-Q_0G(z_0)]N^2_{se}$, which is the parameter of static stability allowing of the effect of cumulus convection. In the following calculation, we assume $Q_0\cong1.14$, $G(z_0)=\sin\pi\frac{z_0}{H}$, where H is the height of tropopause.

In the same way as Ooyama (1966) and Hoskins (1974) did in their derivations, we worked out the criterion of the WAVE-CISK conditional symmetric instability in the baroclinic moist atmosphere as follows:

$$\frac{1}{R_i^*}>\left(1-Q_0\sin\pi\frac{z_0}{H}\right)\frac{N^2_{se}}{N^2}\frac{S^2}{S^2_{se}} \tag{11}$$

$$\text{or}\quad (N^2_{se1}F^2-S^2S^2_{se})<0,$$

where $R_i^*=F^2N^2/S^4$. It can be seen from (11) that the criterion of instability in the dry atmosphere is different from that in the moist atmosphere, so that in the former case, it should be $1/R_i^*>1$ $(N^2_{se}/N^2=1,\ S^2/S^2_{se}=1)$. Therefore, before the occurrence of the convection, the criterion (11) is easy to be satisfied in the neutral or weakly stable stratification atmosphere when $S^2<0\left(\frac{\partial\bar{U}}{\partial z}>0\right)$, $S^2_{se}<0\left(\frac{\partial\bar{\theta}_{se}}{\partial y}<0\right)$, $F^2>0$, which accounts for the occurrence of the convection. Then, considering the effect of the cumulus convection condensation heating,

$(1-Q_0\sin\pi\frac{z_0}{H})$ is a correction to the unstable criterion. In the meantime, a thin layer such as the layers near $z_0=\frac{H}{2}$ can be found to make $\left(1-Q_0\sin\pi\frac{z_0}{H}\right)<0$. The effect of cumulus convection in the WAVE-CISK causes unstable disturbance when $F^2>0$ and $N^2_{Se}<0$; while it restrains the development of the convection when $F^2>0$ and $N^2_{Se}<0$.

3. *Selective Mechanism of the Moist Unstable Wave-Length of Disturbance*

Considering $\nu_y\frac{\partial^2}{\partial z^2}\gg\nu_x\frac{\partial^2}{\partial z^2}$, we can write (10) as

$$\left(\frac{\partial}{\partial t}-\nu_y\frac{\partial^2}{\partial y^2}\right)^2\left(\frac{\partial^2}{\partial y^2}+\frac{\partial^2}{\partial z^2}\right)\psi=-N^2_{Se}\frac{\partial^2\psi}{\partial y^2}+(S^2+S^2_{Se})\frac{\partial^2\psi}{\partial y\partial z}$$
$$-F^2\frac{\partial^2\psi}{\partial z^2}+N^2_{Se}Q_0G(z_0)\left(\frac{\partial^2\psi}{\partial y^2}\right)_{z=z_0}. \tag{12}$$

With $\psi=\Psi(z)e^{ikx+ly}$ and subsequent transformation, we have

$$A\frac{d^2\Psi}{dz^2}+B\frac{d\Psi}{dz}+C\Psi=D\sin\pi\frac{z_0}{H}, \tag{13}$$

where $A=(\sigma+\nu_y k^2)+F^2$, $B=-ik(S^2-S^2_{Se})$,
$C=-K[(\sigma+\nu_y k)+N^2_{Se}]$, $D=N^2_{Se}Q_0(-k^2)\Psi|_{z=z_0}$.

Equation (13) can be regarded as a nonhomogeneous differential equation with constant coefficients when solved at a given σ, k value. Its solution is

$$\Psi=e^{\alpha z}(C_1\cos\beta z-C_2\sin\beta z)+\frac{D}{\left(-B\frac{\pi}{H}\right)^2+\left[C-A\left(\frac{\pi}{H}\right)^2\right]^2}\cdot\left\{\left[C-A\left(\frac{\pi}{H}\right)^2\right]\cdot\sin\pi\frac{z_0}{H}\right.$$
$$\left.-B\frac{\pi}{H}\cos\pi\frac{z_0}{H}\right\}, \tag{14}$$

where α,β are the real and the imaginary roots of $\frac{-B\pm\sqrt{B^2-4AC}}{2A}$, respectively. In order to solve the stream function Ψ, the boundary condition in the vertical direction is taken to be $\Psi|_{z=z_0}=0,\Psi|_{z=H}=0$. Thus we can determine C_1 and C_2 in the solution.

Let $z=z_0$ (taking the top of the boundary layer) to solve for σ with only its real part, and we get

$$\sigma=\left\{\frac{1}{K^2-\left(\frac{\pi}{H}\right)^2}\left[\left(\frac{1}{2}Q_0\sin\frac{\pi}{H}z_0-1\right)K^2N^2_{Se}\right.\right.$$
$$\left.\left.+\sqrt{N^4_{Se}Q_0K^2\sin\frac{\pi}{H}z_0-4\left(\frac{\pi}{H}\right)^2(S^2+S^2_{Se})(-K^2)}-F^2\left(\frac{\pi}{H}\right)^2\right]\right\}^{1/2}-\nu_yK^2. \tag{15}$$

This is a representation of the relation between the growth rate and the wave-length selection. Having selected the above parameters, we can discuss the relation between the wavelength and the other parameters.

(1) *The effect of the viscosity coefficients*

Let $\nu=0.5\times10^{4}m^{2}$/sec or $\nu=2\times10^{4}m^{2}$/sec, $N_{se}^{2}=0.77\times10^{-5}$, $S^{2}=-0.22\times10^{-6}$, $S_{se}^{2}=0.12\times10^{-5}$ and $F^{2}=0.27\times10^{-8}$ ($R_i\cong1$ at the time), and we can calculate σ by using (15). As shown in Fig. 5 (dashed line), the growth rate declines when ν increases and hence the moist unstable wave-length of disturbance increases; otherwise the growth rate of short-wave increases sharply. If $\nu=0$, the most unstable disturbance will be of convective scale, which is identical to that in the dry atmosphere.

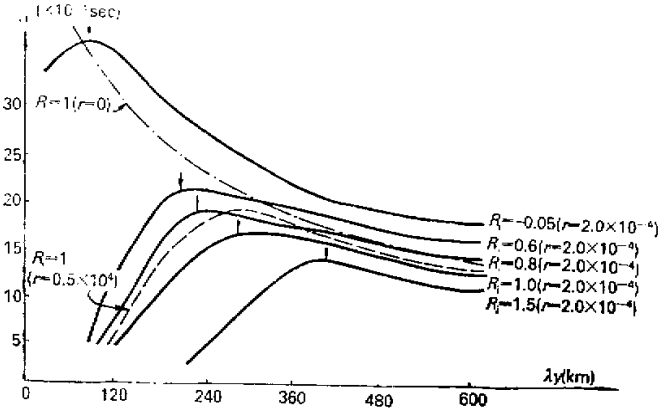

Fig. 5. The relationship between the growth rate and the wave length. ↓: position of the moist unstable wave.

(2) *The effect of* R_i *number* $\left(R_i=\dfrac{g}{\bar{\theta}_{se}}\dfrac{\partial\bar{\theta}_{se}}{\partial z}\Big/\left(\dfrac{\partial u}{\partial z}\right)^{2}\right)$

The R_i number depends upon stratification stability and vertical wind shear. Equation (15) shows that the wave length of the most unstable disturbance becomes longer with the increasing of R_i number. When the R_i number approaches 1, the disturbance is of meso-α-scale. For example, the wave length of the most unstable disturbance is 210 km when R_i number=0.6; it is 300 km when $R_i=1$, with $\nu=2.0\times10^{4}m^{2}$/sec; and the others are the same as (1). The conditional instability stratification is usually found in the meiyu front atmosphere. In this case, the disturbance moves toward the short-wave; the more unstable the stratification, the shorter the wave length (see the solid lines in Fig. 5). The R_i number decreases and the disturbance wave-length reduces because the vertical shear increases near the jet axis when a low-level jet is present.

(3) *The effect of potential pseudo-equivalent temperature and the westerly component*

The formula (11) contains the horizontal gradient of potential pseudo-equivalent temperature, which it is advantageous to the development of disturbance when $S_{se}^{2}<0$ (θ_{se} declines toward north) and $U_g>0$. The results of (15) also show that the scale of developing disturbance is of meso-α. The effect of westerly component on the development of disturbance confirms the conclusion by Bennetts (1979), that is, the inertial instability

develops when $F^2<0$ and the value of F^2 is of little significance for the selection of wave length.

Therefore, when the meiyu front atmosphere satisfies Eq. (11), we can put the appropriate scales of disturbance in the dominant place through the interreaction of physical parameters.

For instance, on 27 June 1981, the atmospheric stratification over the meiyu front was conditionally unstable below 500 hPa ($R_i<0$); almost neutral near 500 hPa ($R_i\sim 0$–3); and stable above 500 hPa ($R_i>10$). Based on Eq. (11) we have calculated the longitudinal distribution of instability criterion. Table 2 gives the latitudinal mean value between 525–475 hPa at 0500Z.

Table 2. The Distribution of Values of Instability Criterion at 0500Z

Region	R_i	$\frac{\Delta\bar{\theta}_{se}}{\Delta z}$	$\frac{\Delta\bar{u}}{\Delta z}$	$\frac{\Delta\bar{\theta}_{se}}{\Delta y}$	$\frac{\Delta\bar{u}}{\Delta y}$	$N^2_{se}F^2-S^2S^2_{se}$
Northern Rain-Band	0—3	2—3	4—5	−3—−5	3	<0
No-Rain Region	2	2	3—5	−0.5	−2	>0
Southern Rain-Band	1—5	0—1	−1	4	2	<0

It can be seen that both the northern and the southern rain-bands satisfy Eq. (11), especially the northern rain-band. If Q_0 is greater (i.e. to intensify appropriately the effect of the latent heating of cumulus convection), the no-rain region also satisfies Eq. (11). From the averaged R_i number, it can be seen that the wave length of disturbance is of meso-α-scale (300–400 km). All this confirms the theoretical discussion.

Part I of the present study has given the cross-section of longitudinal circulation and shows that the disturbance wave length is relatively longer above 500 hPa. There are two roller-like circulations below 500 hPa. the axes of which are parallel to the rain-bands with an interval of about 300 km. The rain-bands correspond to the ascending flow.

IV. CONCLUSIONS

Synthesizing the analyses in Part I and II we come to the conclusions as follows:

1. The non-uniform precipitation area of meiyu front consists of 1–2 meso-α-scale rain-bands. There exists an alternating change in intensity between the two rain-bands.

2. The meso-α-scale rain-bands match the meso-α-scale convergence lines which are the quasi-stationary front at the surface. The distribution of the convergence lines tilts toward north vertically, and further above it sometimes toward south. The meso-α-scale convergence lines associated with an obvious horizontal temperature gradient in the boundary layer but the dew-point horizontal gradient can extend up to the middle and higher troposphere.

3. The convergence in the low-level matches the cyclonic vorticity and it is divergent at the high-level during the development of meso-α-scale rain-bands. Hence there is an ascending motion over the rain-bands and the flow field is disadvantageous to the development of severe convection when the rain-bands decline. The ascending branch of the upper-air jet front circulation overlaps that of the middle-and low-level frontal zone circulation when a single rain-band is developing, which results in the deep convection. There exist the roller-shaped circulations, of which the axes are parallel to the rain-bands at the middle- and low-level, when the double rain-bands are developing. This kind of circulation is associated with the conditional symmetric instability. The WAVE-CISK impels the development of instability.

The wave-length selection of the joint instability is related to the R_i number of the meiyu front atmosphere. To determine appropriate physical parameters, we can put the latitudinal disturbance of meso-α-scale in the dominant place in the development of instability.

4. The alternating change of the double rain-bands in intensity is closely interrelated with that of the moist potential vorticities. The change rate of moist potential vorticity is chiefly determined by its horizontal and vertical divergence as well as the mass flux transport of cumulus. However, the horizontal and vertical divergence of moist potential vorticity of different rain-bands is quite opposite in sign, which constitutes the mechanism of potential vorticity transport of the secondary circulation. The variation of moist potential vorticity is of evident significance for the weather forecasting.

The authors are grateful to Shen Xinyong, Zhang Yin and Liu Zhonghui for assisting in the calculations involved in this paper, and to Yu Zhihao, associate professor of Nanjing University, for offering valuable advice.

REFERENCES

Bennetts, D.A. et al. (1979), Conditional symmetric instability-a possible explanation for frontal rainbands, *Quart. J.R. Met. Soc.*, **105**:945–962.

Browning, K.A. et al. (1969), Air motion and precipitation growth in a wave depression, *Quart. J.R. Met. Soc.*, **95**:288–309.

Elliott, R.D. et al. (1964), On convective bands within Pacific coast storms and their relation to storm structure, *J. Appl. Met.*, **3**:143–154.

Elliott, R.D. et al. (1965), Heat, water and vorticity balance in front zones, *J. Appl. Met.*, **4**:196–211.

Emanuel, K.A. (1981), Inertial instability and mesoscale convective systems. Part 2: Symmetric CISK in a baroclinic flow, *J.A.S.*, **39**:1080–1097.

Hoskins, B.J. (1974), The role of potential vorticity in symmetric stability and instability, *Quart. J.R. Met. Soc.*, **100**:480–482.

Kreitzburg, C.W. et al. (1970), Mesoscale weather systems within an occlusion, *J. Appli. Met.*, **9**:417–432.

Nozumi, Y. et al. (1968), Prefrontal rainbands located in the warm sector of subtropical cyclones over the ocean, *J. Geoph. Res.*, **73**:483–492.

Ooyama, K. (1966), On the stability of baroclinic circular vortex: a sufficient criterion for instability, *J.A.S.*, **23**: 43–53.

Wang Yongzhong et al. (1984), Heavy rain and potential vorticity of current field in lower layer, *Scientia Atmospherica Sinica*, **8**:411–417. (in Chinese with English abstract)

Yang Dasheng et al. (1981), Potential vorticity of monsoonal low-level flows, *J.A.S.*, **38**:2676–2685.

Zhu Baozheng. (1980), A radiative heat scheme for mathematical forecast model, The collected papers of second national mathematical forecasting conference, Science Press, Beijing, China (in Chinese).